Atmospheric Correction of Sentinel-2 Images Using Deep Learning

Stavan Shah[1][a], Kahaan Patel[1][b], Ankur Garg[2][c] and Shivangi Surati[1][d]
[1]*Computer Science and Engineering, School of Technology, Pandit Deendayal Energy University, Gandhinagar, Gujarat, India*
[2]*Indian Space Research Organization, Ahmedabad, Gujarat, India*
{stavanshah20, kahaanpatel5}@gmail.com, agarg@sac.isro.gov.in, shivangi.surati@gmail.com

Keywords: Atmospheric Correction, Pix2Pix, Conditional Generative Adversarial Network, Remote Sensing, Deep Learning, Sentinel-2

Abstract: Remote sensing relies heavily on pre-processing steps, one of which is the Atmospheric Correction (AC). It corrects the effects of atmosphere on satellite images. This makes it a vital step in ensuring accurate estimation of land Surface Reflectance (SR) that can be used in various downstream applications. But such conventional AC methods are computationally expensive because they use physics-based radiative transfer codes, need metadata from each image as well as many different atmospheric parameters which might not all be easy to estimate accurately. A novel Deep Learning (DL) model designed for AC without having to explicitly estimate atmospheric parameters is proposed in this research. The deep learning model was trained using a wide-ranging dataset collected by Google Earth Engine that included four bands of Sentinel 2 images covering all states in India. The proposed approach directly predicts SR values from Sentinel-2 satellite imagery using this data driven method. It generated promising results by accurately estimating SR values with ground measurements and sentinel input data experiments confirming this point too. This approach not only simplifies the AC process but also achieves comparable or even superior performance compared to traditional physics-based methods. The evaluation results show that Pix2Pix model has good performance, with average SSIM, PSNR, RMSE and MAE of 0.96, 42.14, 0.0097 and 0.0071 respectively. The experimental findings underscore the potential of deep learning as a robust and efficient alternative for atmospheric correction in remote sensing applications.

1 INTRODUCTION

Through remote sensing, the images taken from above the earth's surface are essential for monitoring and understanding. Unfortunately, these images are normally tainted with atmospheric effects such as scattering and absorption that can distort actual surface reflectance. Atmospheric correction is a critical pre-processing step in remote sensing that aims at removing these atmospheric influences to give precise values of surface reflectance (Zhu and Xia, 2023), (Zhang et al., 2022). The main objective of AC is to transform Top-Of-Atmosphere (TOA) reflectances into Bottom-Of-Atmosphere (BOA)/surface reflectances. This enables interpretation and investigation of remote sensing data more accurately. Complex mathematical formulation involving the aerosol content, Rayleigh scattering as well as water vapor among others are necessary to convert TOA Reflectance to SR. An example includes 6S (Second Simulation of the Satellite Signal in the Solar Spectrum) model that is used to approximate atmospheric parameters depending on radiative transfer principles (Ilori and Knudby, 2020). Particles such as atmospheric gases, aerosols and others scatter and absorb sunlight and hence, the process of atmospheric correction is extremely important for any satellite imagery analysis.

The Sentinel-2 mission is outstanding among the numerous Earth observation satellites due to its extensive coverage and high resolution. It belongs to Copernicus program of European Space Agency and offers multispectral imagery with 13 spectral bands across visible, near infrared and short wavelength infrared parts of electromagnetic spectrum. These are useful in land cover characterization, vegetation indices retrieval and water quality monitoring thus mak-

[a] https://orcid.org/0009-0000-1778-1745
[b] https://orcid.org/0009-0005-9981-6257
[c] https://orcid.org/0000-0002-2872-5690
[d] https://orcid.org/0000-0003-4381-5130

Shah, S., Patel, K., Garg, A. and Surati, S.
Atmospheric Correction of Sentinel-2 Images Using Deep Learning.
DOI: 10.5220/0013303900004646

In *Proceedings of the 1st International Conference on Cognitive & Cloud Computing (IC3Com 2024)*, pages 175-185
ISBN: 978-989-758-739-9

ing the Sentinel-2 data paramount in various environmental and agriculture applications (Phiri et al., 2020).

These methods are usually based on physics which require extensive computational resources and accurate knowledge of the atmosphere variables (Liu et al., 2022). In the recent years Pix2Pix model, a GAN variant, has achieved impressive results in image-to-image translation tasks. In the proposed work, while trained on large paired datasets of TOA and SR images for instance, Pix2Pix models generate high-quality SR images directly from TOA inputs by learning their complex mapping. The other advantages of using this model is flexibility, direct optimization through end-to-end learning framework, generalization competencies and robustness to deviations in input data and high quality outputs. The generated images are then compared using several evaluation parameters such as Structural Similarity Index Measure (SSIM), Peak Signal to Noise Ratio (PSNR), Root Mean Square Error (RMSE), and Mean Absolute Error (MAE) with their ground truths.

The organization of the paper is as follows. The detailed discussion of prior methods and techniques of atmospheric correction is presented in Section 2. The data, model architecture and evaluation techniques incorporated in this work are presented in Section 3. The evaluated results of the proposed methodology are presented and discussed in section 4. Section 5 wraps up by summarising the main conclusions and going over the probable next lines of research.

2 RELATED WORK

Several algorithms for Aerosol Optical Depth (AOD) retrieval from TOA data have been developed and are widely used. Some of these algorithms are Dark Target (Remer et al., 2020), Deep Blue (Hsu et al., 2013) and Multi-Angle Implementation of Atmospheric Correction (MAIAC). However, one of the main issues in AOD retrieval is the difficulty in accurately parameterizing the basic aerosol optical properties which leads to large uncertainties. Additionally, there exist other methods used for Columnar Water Vapor (CWV) estimation. Some common approaches include Low-Rank Subspace Projection-Based Water Estimator (LRP-WAVE) (Acito and Diani, 2018) and Atmospheric Pre-corrected Differential Absorption (APDA) (Schläpfer et al., 1998). Nevertheless, these algorithms suffer from drawbacks such as being based on physical assumptions or requiring hard-to-get parameters respectively. SR uncertainty comes from two factors; AOD and CWV estimated errors during SR derivation from TOA data estimation, AODs alone should not be a priority compared to both because their accuracies affect each other's accuracy too much and hence, they need accurate estimates.

On the flip side, image-based methods achieve AC solely through the use of images taken from satellite or aerial sensors; they don't need any atmospheric parameters as input but instead utilize only the information inherent in the image itself. The Dark Object Subtraction is one of the most basic techniques in which at least two targets with low and high reflectivity from within scene must be identified. Another image-based AC model called Quick Atmospheric Correction (QuAC) (Bernstein et al., 2012) works on a different assumption- average group material spectra remains same across various scenes. If there are more than ten different things present in background then QuAC performs well. Although they are intuitive and computationally efficient, these methods lack ability to quickly estimate surface reflectance values at first order due to their accuracy under conditions involving seasonal and spectral variation.

Based on deep learning model approaches, two atmospheric correction deep learning models were trained and evaluated using one hundred thousand batches of 40 transformed reflectance spectra to radiance by means of MODTRAN (Basener and Basener, 2023). It allowed the deep learning model to figure out the physics of radiation transfer from MODTRAN. For this purpose, they compared two methods to estimate corrections in a well-known QuAC model which is based on constant mean endmember reflectance assumption. Using the HY-1C CZI as a case study, a new approach is presented in (Zhao et al., 2023) to atmospheric correction based on deep learning (SSACNet). The third dimension convolution was applied to extract spatial and spectral features for the image while second dimension convolution was investigated for recovery of lost spatial information. According to in-situ data, the SSACNet shows decent performance having average correlation coefficient of 0.89 and Absolute Percentage Deviation (APD) ranging from 21.53% to 35.41% in four bands.

To do AC, all deep learning models that could match the efficiency and accuracy of physics-based techniques in computing are observed. Additionally, DL models do not need any climatic or geometric parameters as input. Compared to those based on physics, computational power usage is reduced with DL models. This is because, they can learn features automatically and thus, making it easy to build and train models. Stacked autoencoders, Convolutional Neural Networks (CNNs) (Wang et al., 2022), and vision transformers (Liu et al., 2024) are some promising methods used in remote sensing imaging applications such as spectral spatial and temporal feature extraction being performed by them.

In the proposed work, a new method is described that uses DL for atmospheric correction in remote sensing data without the need for atmospheric parameters and geometric parameters; only input images are considered. To the best of our knowledge, the proposed methodology is the first approach that utilizes Pix2Pix model for AC. The deep learning Pix2Pix model was developed using a large dataset from different states of India in order to improve its performance and generalization.

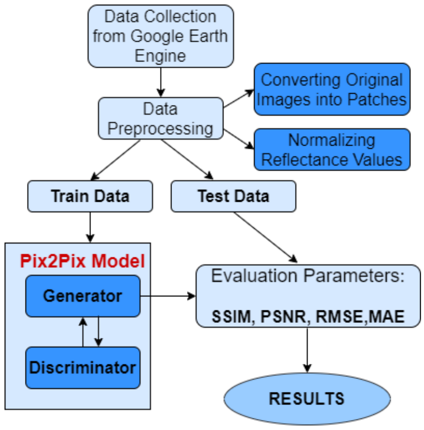

Figure 1: Model flowchart.

3 PROPOSED METHODOLOGY

The flowchart presented in Figure 1 outlines the steps of proposed methodology for atmospheric correction of sentinel-2 images.

3.1 Dataset Collection

The proposed research used data from Google Earth Engine, a cloud-based platform that provides access to a wide range of geographical datasets and satellite images. Both atmospherically corrected and incorrected satellite images were gathered for this study. Atmospherically incorrected images are TOA measurements taken by satellite sensors without compensating for scattering or absorption by atmosphere. Atmospherically corrected pictures have been processed to eliminate atmospheric interference so that surface reflectance values accurately represent features on earth's surface.

In this study, Sentinel-2 satellite data from the Google Earth Engine is used. Sentinel-2 is a European Space Agency (ESA) satellite mission designed for monitoring Earth's land and coastal areas. The usual number of spectral bands in Sentinel 2A/B MSI imagery is 13 bands. However, only four specific bands having 10m resolution were included in this study as shown in Table 1.

Table 1: Sentinel-2 Band Information.

Band	**Wavelength (nm)**	**Resolution (m)**
Band 2 (Blue) (b)	490	10
Band 3 (Green) (g)	560	10
Band 4 (Red) (r)	665	10
Band 8 (Near-Infrared) (vnir)	842	10

A total of 1000 images were collected. Each image is atmospherically incorrected and its respective atmospherically corrected image mapped together in order to perform image to image translation. The images cover various regions across India, providing a diverse and representative sample for analysis. There are two ways to visualize the data:

1. True color composite: In true color composite imagery, the red, green, and blue bands (Bands 4, 3, and 2 respectively) are combined to replicate human vision, producing an image akin to what the human eye perceives. RGB images (true color composite) are visualized in Figure 2a, where (1), (3) are Atmospherically Incorrected Images whereas (2), (4) are their Atmospherically Corrected Images respectively.
2. False color composite: False color composite utilizes non-visible bands, typically near-infrared (Band 8), red (Band 4), and green (Band 3), to highlight features not discernible to the human eye. This composite reveals vegetation health, land-water boundaries, and other environmental characteristics, enhancing analysis in applications such as agriculture, forestry, and environmental monitoring. The False color images composite of 2 sample data are visualized in Figure 2b, where (1) and (3) are Atmospherically Incorrected Images whereas (2) and (4) are their Atmospherically Corrected Images respectively.

3.2 Data Preprocessing

After gathering data from Google Earth Engine, original dataset consisted of images in different sizes like 1000x1000 and 1200x1200 pixels. These patches were taken out from input (atmospherically incorrected) and ground truth (atmospherically corrected) images both at 256x256 pixels to standardize input

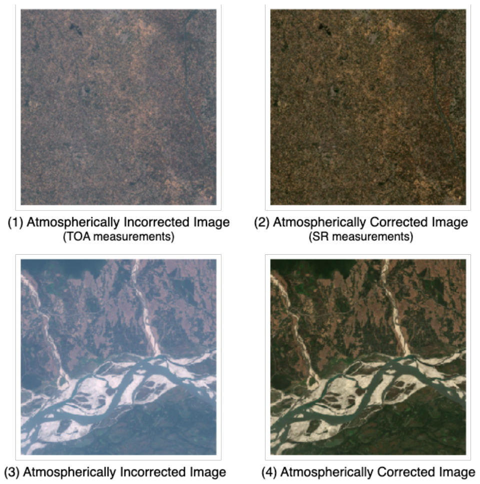

(a) True color composites.

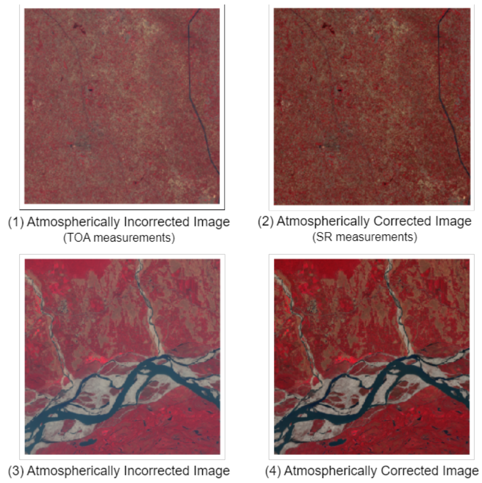

(b) False color composites.

Figure 2: Comparison of true and false color composites.

data for further analysis and processing. Hence, each image irrespective of its original dimensions became (256, 256, 4) where '4' refers to four bands denoting red, green, blue and near-infrared channels. In addition, top of atmosphere and surface reflectance measurements obtained through satellite imagery usually range between 0-30000.

Each measurement was divided by 10000 as an important preprocessing step because this normalization process has several benefits such as scaling pixel values into standard range so that they can be consistently compared across different images; secondly during training ML algorithms tend to work more stable and converge faster when their pixel values are normalized over smaller ranges. Moreover, the collected dataset was split into two sets: training set and testing set. Among 1000 images, 800 were employed for model training while remaining 200 served as test data.

3.3 Model Architecture

In the field of transforming pictures into other pictures, Pix2Pix model is a very important and useful tool. It provides a strong method for converting input images to desired outputs which supports different applications like image denoising, style transfer or semantic segmentation. For satellite imagery atmospheric correction, this model can be used to convert atmospherically incorrected images (rep-resenting top of atmosphere measurements) into atmospherically corrected (depicting surface reflectance measurements) that is vital for improving the quality and accuracy of satellite image analysis. The structure of the Pix2Pix model includes two major parts as discussed.

3.3.1 Generator

The generator usually takes as input the images with incorrect atmosphere corrections (TOA measurements), which are typically represented as tensors of shape (256, 256, 4) as shown in Figure 3. The role of the generator is to convert input images (atmospherically incorrected images representing TOA measurements) into desired outputs (atmospheric corrected images representing SR measurements). The architecture of this generator is designed such that it can collect and elaborate upon spatial as well as spectral characteristics present in input images while delivering accurate results that are visually pleasing. Structure of a generator involves downsampling and upsampling parts for extracting abstract features from input images and generating output ones correspondingly (Figure 3). In Pix2Pix model's generator, an altered version U-Net architecture was used that is efficient and widely adopted in neural network design for image-to-image translation tasks. This alteration includes encoder-decoder framework with skip connections enabling both down-sampling and up-sampling operations while keeping intact spatial information preservation capabilities within them.

Generator has two main layers:

1. Encoder: The encoder of the Pix2Pix model is composed of various blocks where each block contains a convolutional layer, batch normalization and Leaky ReLU activation function. This arrangement enables the encoder to extract high-level features from input images effectively as it reduces their spatial dimensions progressively.

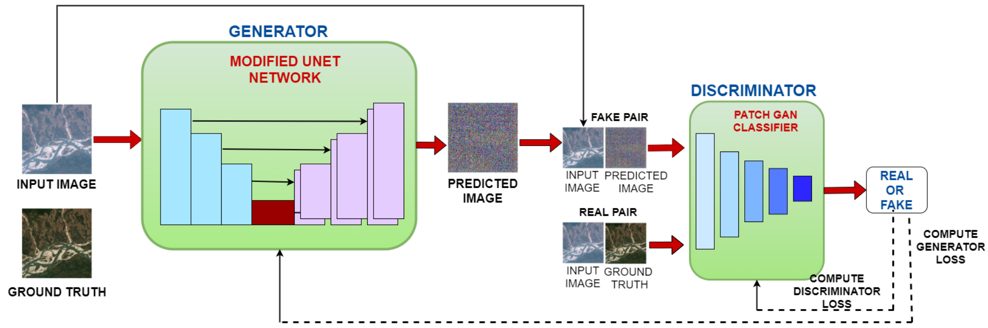

Figure 3: Pix2Pix architecture.

Each layer in this part consists of:

- Convolutional Layer: Every block begins with a convolutional layer that applies a set of learnable filters to the input feature. These filters are designed to capture spatial information and local patterns present in input images, thus promoting feature extraction and representation learning.
- Batch Normalization: The activations for each layer across the mini-batch are stabilized by applying batch normalization after the convolutional layer.
- Leaky ReLU Activation: After batch normalization, applying a Leaky ReLU activation function brings non-linearity into model that helps it capturing complex features. It allows small gradients for negative i/p values that avoids vanishing gradient problem while promoting more stable effective learning.

2. Decoder: The decoder of the Pix2Pix model is made up of a series of blocks that mirror the encoder, which itself consists of transposed convolutional layers along with batch normalization, dropout (used in the first 3 blocks), and ReLU activation. This also includes skip connections between corresponding encoder and decoder blocks to allow information to move through the system more easily while retaining spatial details. Each decoder layer has:

   - Transposed Convolutional Layer: Each block in the decoder begins with a transposed convolutional layer, or deconvolution/upsampling layer. It enlarges input feature maps so that higher resolution output images can be reconstructed by the decoder.
   - Batch Normalization: Activations are stabilized and training is speed up by applying batch normalization after the transposed convolutional layer.
   - Dropout (Applied to the First 3 Blocks): Overfitting is prevented and generalizability enhanced by applying dropout to first three blocks in the decoder.
   - ReLU Activation: Non-linearity is brought about and feature representation heightened following batch normalization through an application of ReLU activation function. Sparse passing of only positive values to next layer(s) promoted by ReLU.

Allowing the model to retain and propagate important spatial information throughout the network, skip connections between encoder and decoder blocks (as pictured in Figure 4) help in generating output images with fine-grained details during reconstruction. In fact the shown design of U-Net like this one also guarantees that during image-to-image translation process by Pix2Pix; spatial features are captured or preserved effectively at all levels of resolution.

The architecture of generator model is shown in Figure 4, where first half acts as an encoder which downsamples input image size while second part acts as a decoder which upsamples it back again with skip connections between them.

3.3.2 Discriminator

In the Pix2Pix conditional generative adversarial network, a discriminator acts as a convolutional PatchGAN classifier, which means that it is designed to tell apart real image patches from fake ones. During adversarial training, it provides the generator with feedback about how well it creates natural-looking images. Every block in the discriminator performs a sequence of operations (Figure 5): Convolution, Batch Normalization, Zero Padding (in some layers), Leaky ReLU activation. This design allows the discriminator to extract features from image patches and learn discriminative representations for classification. After the last layer of the discriminator, there is an output shaped as follows: (batch-size, 30, 30, 1). In this

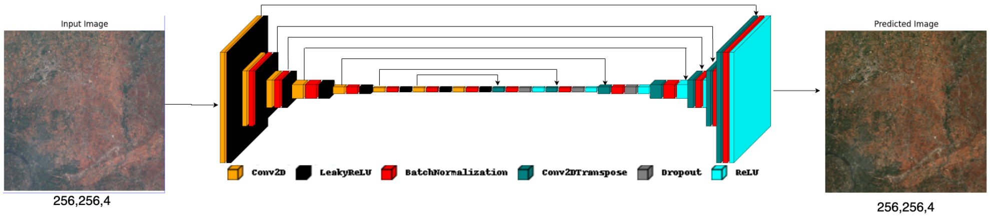

Figure 4: Generator architecture.

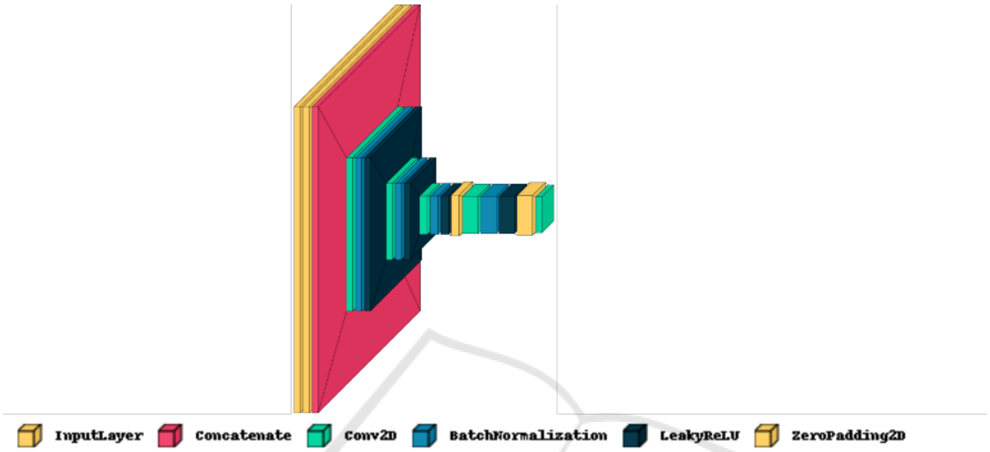

Figure 5: Discriminator architecture.

case, each 30 x 30 image patch classifies a 70 x 70 section of the in-put image. Such patch-wise classification strategy lets the discriminator concentrate on local image details instead of global ones, thus making it more effective for image-to-image translation tasks. The discriminator receives two inputs as shown in Figure 3:

1. Real Pair: Input image (atmospherically incorrected image) and target image (atmospherically corrected image), which should be classified real by discriminator.
2. Fake Pair: The input image (atmospherically incorrected image) and the generated image (image generated by generator), which should be classified as fake by it.

In order to process these inputs, they are concatenated along channel axis using tf.concat([inp, tar], axis= -1) so that a composite input containing both input images as well as corresponding ground truth images/generated images can be created.

By making use of this joint input, discriminator becomes able to distinguish between real and fake pairs of images thereby giving adversarial feedback to generator which in turn helps it produce more believable output pictures. Through this back-and-forth between generator and discriminator components within Pix2Pix model itself learns how make good translations among different types of pictures while at same time ensuring that all atmospherically wrong-looking inputs get transformed into atmospherically right ones. Discriminator architecture is presented in Figure 5 below where first two layers represent input images being concatenated in second layer (pink layer). Various operations performed on concatenated pair are depicted in Figure 5.

3.4 Model Training

The training steps can be divided into several important parts which serve to improve the robustness as well as accuracy of deep learning models.

1. Loss Functions: In Pix2Pix, the generator loss involves multiple components that are useful for guiding the training process. These components are such as:
   - L1 Loss: This measures the difference between pixels in generated images and those in original images also called Mean Absolute Error (MAE) loss.

$$\text{L1 Loss} = \frac{1}{N}\sum_{i=1}^{N}|G(x_i) - y_i| \tag{1}$$

   - Generator GAN Loss: It is derived through an adversarial training process based on discriminator output which measures how good or bad our generated samples are when compared against real ones.

$$\mathcal{L}_{\mathcal{G}} = -\mathbb{E}_z[\log(D(G(z)))] \quad (2)$$

- Generator Total Loss: This is aggregate of L1 loss with a weighted generator GAN loss. Goal is to balance image fidelity and image realism during training.

$$\text{Gen Total Loss} = \text{L1 Loss} + \lambda \cdot \text{Gen GAN Loss} \quad (3)$$

- Discriminator Loss: The discriminator loss function measures the discrepancy between the discriminator's predictions (probability scores) and the ground truth labels (real or fake).

$$\text{Discriminator Loss} = -\frac{1}{N}\sum_{i=1}^{N}[y_i \log(D(x_i)) + (1-y_i)\log(1-D(x_i))] \quad (4)$$

2. Optimization Algorithm: The Adam optimizer was used to train our deep learning model with a learning rate of 0.0002. It ensures fast convergence and optimization by gradient descent. Adam's adaptive learning rate mechanism that adjusts based on the first and second moments of the gradients, provides a balance between convergence speed and stability, crucial for the adversarial nature of GANs. This adaptability helps in achieving faster convergence and handling the complex, non-linear transformations required for atmospheric correction, where pixel-wise accuracy is critical. Momentum in Adam further smooths the optimization path, leading to more stable and reliable training outcomes. A learning rate of 0.0002 has been empirically validated across various implementations of GANs, including Pix2Pix, ensuring high quality image generation. This effectively balances need for quick convergence without sacrificing stability, avoiding the pitfalls of divergence seen with higher rates and the slow training of lower rates. The robustness of Adam to noisy gradients, a common challenge in GAN training, enhances its suitability for atmospheric correction, ensuring consistent and accurate correction across diverse atmospheric conditions and geographical regions.
3. Batch Processing and Summary: Mini-batch stochastic gradient descent was applied throughout training, using a batch size of 2. This approach helps save memory space while speeding up the training process. The model parameters are updated based on small subsets of the training data. Furthermore, a summary after every 10 epochs is created that include model predictions on three randomly selected images from dataset using checkpointed model at that epoch. At these checkpoints, both the Generator and Discriminator models were saved to preserve their progress in training.
4. Epochs and Early Stopping: Training lasted for 100 epochs (equivalent to 80,000 steps) but had an early stopping criterion based on validation loss to avoid overfitting network weights. With early stopping, one can monitor how well the model performs during training and stop when there is no improvement in validation performance.

3.5 Evaluation Parameters

Evaluating model performance is crucial to assess the fidelity and accuracy of the generated images compared to ground truth images (atmospherically corrected). Ground truth images provide a reference for the desired output, allowing us to quantitatively measure the similarity between the generated/predicted images and the true images. The evaluation parameters used for assessing the performance of Pix2Pix model on both the training and testing datasets include:

1. Structural Similarity Index (SSIM): It measures similarity between two images based on their luminance, contrast and structure where difference in perception between generated and ground truth images is measured.

2. Peak Signal-to-Noise Ratio (PSNR): PSNR measures the ratio between the maximum possible power of a signal and the power of corrupting noise that affects the fidelity of its representation. It quantifies the quality of the generated images compared to the ground truth images.

3. Root Mean Squared Error (RMSE): RMSE measures the average difference between values predicted by the model and the observed values. It represents square root of average of the squared differences between predicted and observed values.

4. Mean Absolute Error (MAE): MAE measures the average absolute difference between the predicted and observed values. It provides a more intuitive understanding of the average error magnitude.

4 RESULTS

4.1 Predicting Images on Test Set

The model performed well on the test dataset, producing atmospherically corrected images that were very similar to the corresponding ground truth images. The synthesized image showed features and visual appearances in common with the truth image. It reproduced such things as texture, color tones and structural components correctly which shows that it can capture detailed patterns properly. Such similarity is shown in Figure 6 where predicted (generated) images are compared against their respective input images and inputted ground truths.

4.2 Evaluation Metrics

SSIM, PSNR, RMSE and MAE are used for evaluating quality of generated images compared to ground truth images in image processing tasks. Range of SSIM values is from -1 to 1, where 1 indicates perfect similarity between the images. Good SSIM values typically range between 0.9 and 1, indicating high similarity and good quality. SSIM values below 0.5 are generally considered poor and may indicate significant differences between the images. PSNR values are expressed in decibels (dB). Higher PSNR values indicate better quality, with values closer to infinity representing perfect reconstruction. PSNR values above 30 dB are typically considered good for most applications. PSNR values below 20 dB may indicate significant distortion and poor quality. If the values of both RMSE and MAE are decreasing then it can be considered that difference in pixels of ground truth and generated images is reduced and both the images are getting more similar to each other.

The below tables (Tables 2 and 3) depicts the minimum, maximum, mean and standard deviation of all evaluation parameters. Values in Table 2 are the evaluation parameters that are recorded before training process and in that the images are only generated via Pix2Pix generator model (similar to U-net). Whereas, values in Table 3 are the evaluation parameters that are recorded after 100 epochs of training the Pix2Pix model. There is a significant change in values between these tables. Starting with SSIM, which assesses the similarity between two images, a mean SSIM value of -0.0025 with a standard deviation of 0.0605 is shown in Table 2. This indicates poor matching between the generated and ground truth images before training. In contrast, a significant improvement in SSIM metrics is revealed in Table 3, with a mean value of 0.961 and a standard deviation of 0.068. This substantial enhancement demonstrates the model's ability to produce images that closely resemble the ground truth after training. 95% of SSIM values are greater than 0.85 which indicates that model is efficiently generating images similar to ground truth. SSIM values recorded for test dataset are described in Figure 7a.

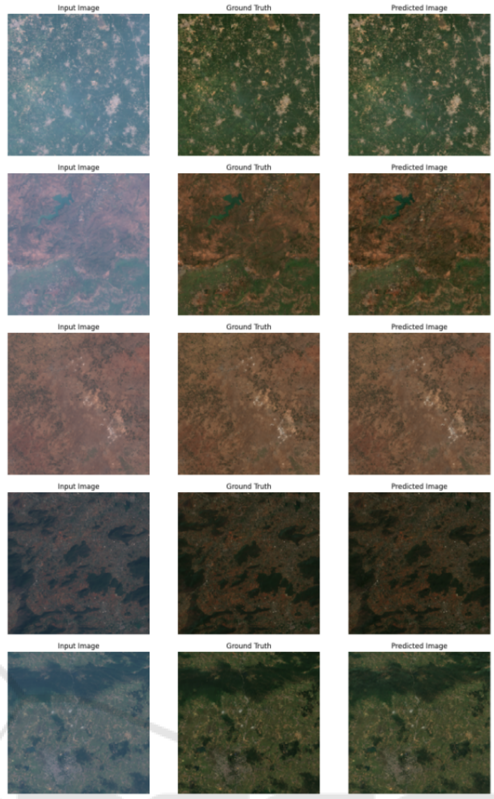

Figure 6: Generated images.

Moving on to PSNR, Table 2 demonstrates a mean PSNR value of 11.0188 dB with a standard deviation of 0.6115 dB. These values indicate low image quality before training, as higher PSNR values correspond to better image fidelity. How-ever, Table 3 shows a remarkable improvement in PSNR metrics, with a mean value of 42.14 dB and a standard deviation of 5.51 dB. The drastic increase in PSNR reflects a significant enhancement in image quality after training, suggesting that the model produces images with reduced noise and improved fidelity. 97.5% of PSNR values are greater than 30 that indicates that model is efficiently generating images similar to ground truth. The PSNR values recorded for test dataset are described in Figure 7b.

Next, Table 2 exhibits mean RMSE and MAE values of 0.281 and 0.219, respectively, with standard deviations of 0.021 and 0.017. These values indicate relatively high errors between generated and

Table 2: Evaluation metrics before training.

Evaluation Parameters	Maximum value	Minimum value	Mean value	Standard Deviation
SSIM	0.00202	-0.0336	-0.0025	0.0605
PSNR	12.663	7.0231	11.0188	0.6115
RMSE	0.445	0.232	0.281	0.021
MAE	0.345	0.161	0.219	0.017

Table 3: Evaluation metrics after training for 100 epochs.

Evaluation Parameters	Maximum value	Minimum value	Mean Value	Standard Deviation
SSIM	0.997	0.563	0.961	0.068
PSNR	52.93	25.11	42.14	5.51
RMSE	0.0555	0.0022	0.0097	0.0075
MAE	0.0394	0.0017	0.0071	0.0051

ground truth images before training. However, Table 3 demonstrates a noticeable reduction in both metrics, with mean values of 0.0097 and 0.0071, and standard deviations of 0.0075 and 0.0051, respectively. This reduction signifies a significant improvement in model's ability to minimize errors between generated and ground truth images after training. Thus, comparison between Tables 2 and 3 highlights substantial improvement in model's performance after 100 epochs of training.

4.3 Interpreting Losses

It takes more finesse to interpret the logs when training a GAN or a conditional GAN like Pix2Pix, compared to simpler models such as classification or regression models. In our training process, several loss functions are employed as dis-cussed in section 3.4. Throughout the training epochs, it's crucial to monitor these losses to ensure balanced training dynamics between the generator and discriminator networks. One key aspect to consider is the behaviour of the Generator L1 Loss, which consistently decreased from epoch 1 to epoch 100 (as shown in Figure 8c). This indicates that the generator network progressively improved its ability to generate images that closely match the ground truth, reflecting the effectiveness of the training process. However, interpreting GAN losses is more complex. If either Generator GAN Loss or Discriminator Loss becomes excessively low, it suggests that one model is overpowering other. Moreover, nature of GAN training involves a competitive process between generator and discriminator. Improvement in one network's loss often corresponds to an increase in other network's loss, creating a cycle of adversarial learning. This dynamic equilibrium results in fluctuating loss values of both networks until converge to stable points. It is observed that both discriminator and generator losses converge to permanent values over time (Figure 8a and 8b). This convergence indicates that training process has reached a stable equilibrium, where neither network dominates other. Achieving this balance is crucial for producing high-quality images that faithfully represent ground truth.

5 CONCLUSIONS

The proposed methodology successfully demonstrated feasibility of extracting surface reflectance values from top-of-atmosphere reflectance values using deep learning technique. Through application of the Pix2Pix model, accurate atmospheric correction is achieved, transforming TOA reflectance images into atmospherically corrected images with remarkable fidelity. The evaluation metrics (Table 3) consistently indicate high-quality results, affirming the effectiveness of the proposed approach. Furthermore, the analysis of loss functions revealed optimal training dynamics, with the model converging to stable values. This suggests robust learning and effective adaptation to the training data. The evaluation results show that Pix2Pix model has good performance, with average SSIM, PSNR, RMSE and MAE of 0.96, 42.14, 0.0097 and 0.0071 respectively. Importantly, the methodology eliminates the need for complex metadata or parameter calibration typically associated with traditional atmospheric correction techniques. By leveraging deep learning, a streamlined and efficient solution for atmospheric correction is provided, offering potential applications in remote sensing and environmental monitoring without the burden of extensive preprocessing.

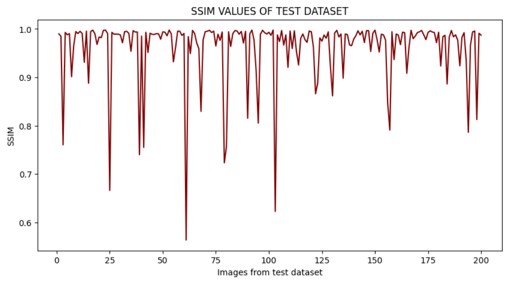

(a) SSIM values.

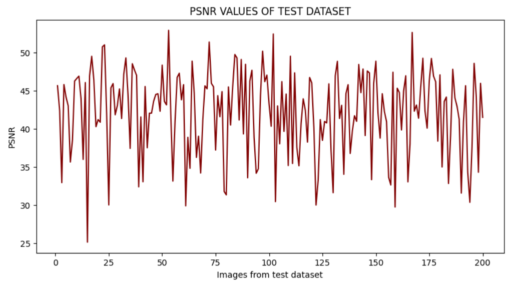

(b) PSNR values.

Figure 7: SSIM and PSNR values between ground truth and predicted images from test dataset.

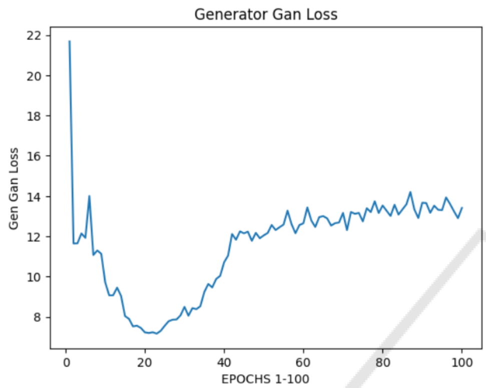

(a) Generator Gan Loss during training.

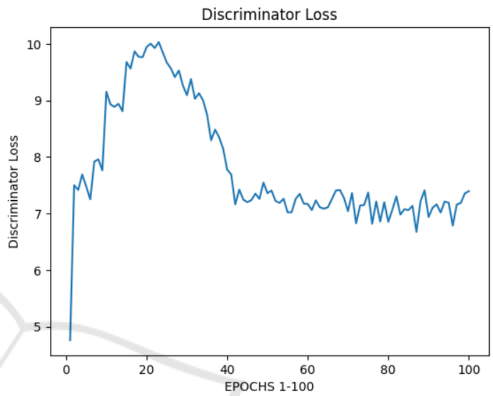

(b) Discriminator Loss during training.

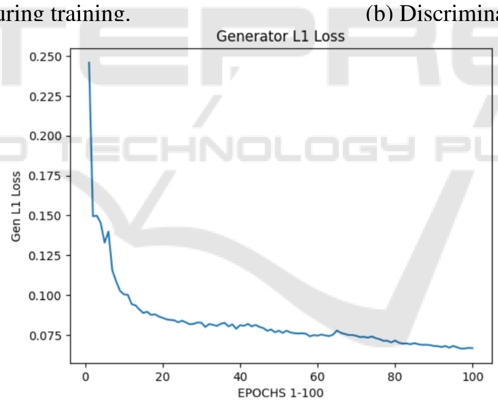

(c) Generator L1 Loss during training.

Figure 8: Comparison of losses.

REFERENCES

Acito, N. and Diani, M. (2018). Atmospheric column water vapor retrieval from hyperspectral vnir data based on low-rank subspace projection. *IEEE Transactions on Geoscience and Remote Sensing*, 56(7):3924–3940.

Basener, B. and Basener, A. (2023). Gaussian process and deep learning atmospheric correction. *Remote Sensing*, 15(3):649.

Bernstein, L. S., Jin, X., Gregor, B., and Adler-Golden, S. M. (2012). Quick atmospheric correction code: algorithm description and recent upgrades. *Optical engineering*, 51(11):111719–111719.

Hsu, N., Jeong, M.-J., Bettenhausen, C., Sayer, A., Hansell, R., Seftor, C., Huang, J., and Tsay, S.-C. (2013). Enhanced deep blue aerosol retrieval algorithm: The second generation. *Journal of Geophysical Research: Atmospheres*, 118(16):9296–9315.

Ilori, C. O. and Knudby, A. (2020). An approach to minimize atmospheric correction error and improve physics-based satellite-derived bathymetry in a coastal environment. *Remote Sensing*, 12(17):2752.

Liu, S., Li, H., Jiang, C., and Feng, J. (2024). Spectral–spatial graph convolutional network with dynamic-synchronized multiscale features for few-shot hyperspectral image classification. *Remote Sensing*, 16(5):895.

Liu, S., Zhang, Y., Zhao, L., Chen, X., Zhou, R., Zheng, F., Li, Z., Li, J., Yang, H., Li, H., et al. (2022). Quantitative and automatic atmospheric correction (quaac): Application and validation. *Sensors*, 22(9):3280.

Phiri, D., Simwanda, M., Salekin, S., Nyirenda, V. R., Murayama, Y., and Ranagalage, M. (2020). Sentinel-2 data for land cover/use mapping: A review. *Remote Sensing*, 12(14):2291.

Remer, L. A., Levy, R. C., Mattoo, S., Tanré, D., Gupta, P., Shi, Y., Sawyer, V., Munchak, L. A., Zhou, Y., Kim, M., et al. (2020). The dark target algorithm for observing the global aerosol system: Past, present, and future. *Remote sensing*, 12(18):2900.

Schläpfer, D., Borel, C. C., Keller, J., and Itten, K. I. (1998). Atmospheric precorrected differential absorption technique to retrieve columnar water vapor. *Remote Sensing of Environment*, 65(3):353–366.

Wang, Y., Hong, D., Sha, J., Gao, L., Liu, L., Zhang, Y., and Rong, X. (2022). Spectral–spatial–temporal transformers for hyperspectral image change detection. *IEEE Transactions on Geoscience and Remote Sensing*, 60:1–14.

Zhang, H., Ma, Y., Zhang, J., Zhao, X., Zhang, X., and Leng, Z. (2022). Atmospheric correction model for water–land boundary adjacency effects in landsat-8 multispectral images and its impact on bathymetric remote sensing. *Remote Sensing*, 14(19):4769.

Zhao, X., Ma, Y., Xiao, Y., Liu, J., Ding, J., Ye, X., and Liu, R. (2023). Atmospheric correction algorithm based on deep learning with spatial-spectral feature constraints for broadband optical satellites: Examples from the hy-1c coastal zone imager. *ISPRS Journal of Photogrammetry and Remote Sensing*, 205:147–162.

Zhu, W. and Xia, W. (2023). Effects of atmospheric correction on remote sensing statistical inference in an aquatic environment. *Remote Sensing*, 15(7):1907.